Physics of Plasmas ARTICLE pubs.aip.org/aip/pop

Electron temperature gradient instability and transport analysis in NSTX and NSTX-U plasmas

Cite as: Phys. Plasmas **32**, 022305 (2025); doi: 10.1063/5.0232697
Submitted: 9 August 2024 · Accepted: 21 December 2024 ·
Published Online: 26 February 2025

View Online Export Citation CrossMark

C. F. Clauser,[1,2,a)] T. Rafiq,[2] J. Parisi,[3] G. Avdeeva,[4] W. Guttenfelder,[3,5] E. Schuster,[2] and C. Wilson[2]

AFFILIATIONS

[1]Plasma Science and Fusion Center, MIT, Cambridge, Massachusetts 02139, USA
[2]Lehigh University, Bethlehem, Pennsylvania 18015, USA
[3]Princeton Plasma Physics Laboratory, Princeton, New Jersey 08540, USA
[4]General Atomics, La Jolla, California 92121, USA
[5]Type One Energy, Oak Ridge, Tennessee 37830, USA

[a)]Author to whom correspondence should be addressed: cclauser@psfc.mit.edu

ABSTRACT

Extensive linear and nonlinear simulations to study electron temperature gradient (ETG) stability and thermal transport in National Spherical Torus Experiment (NSTX) and NSTX-U plasmas were performed using the fully electromagnetic gyrokinetic code CGYRO. Linear simulations were performed to determine ETG thresholds in different discharges, showing that ETG modes in spherical tokamaks can present different scalings compared to conventional aspect-ratio tokamaks. Nonlinear gyrokinetic simulations were conducted for selected cases to calculate electron thermal transport and compare to experimental values. Results are also compared with those of ETG modes in the multi-mode model and the Trapped-Gyro-Landau-Fluid reduced model codes, to better understand their applicability in spherical tokamaks.

I. INTRODUCTION

Experiments on the National Spherical Torus Experiment (NSTX) have demonstrated that electron thermal transport is anomalous and dominates over ion thermal transport, which has been reported to usually be at neoclassical levels.[1,2] One of the modes that is responsible for electron thermal transport is the electron temperature gradient (ETG) mode.[3,4] ETG modes, which are mostly electron-scale, are the usual driving electron thermal transport mechanism when ion-scale turbulence is suppressed. There is now a vast literature about electron-scale turbulence (see for example Ref. 5 and references therein). In particular, ETG may play a significant role in the pedestal of conventional aspect ratio tokamaks where, for example, they were shown to account for a significant fraction of the heat flux on DIII-D[6] and JET,[7] or the ion-scale ETGs that were found to be dominant in a JET discharge.[8] Along with these, there were also efforts in developing reduced models to improve predicting capabilities.[6,9] Conversely, ETG turbulence has been also found to be relevant in spherical tokamaks (STs)[10,11] and, in particular, in NSTX discharges.[12–18] To properly model anomalous transport in tokamaks and, in particular, the transport caused by ETG modes, gyrokinetics is commonly used in spherical tokamaks.[15,19] This includes a validation exercise on NSTX data that showed agreement between electron-scale turbulence with gyrokinetic simulations.[17] However, it is computationally expensive for fast or real-time profile reconstruction and, in some cases, for profile prediction. Therefore, reduced models need to capture ETG physics, namely, thresholds and transport, in order to be used for predicting profiles in present and future devices like NSTX and NSTX-U. Hence, validating these models against gyrokinetic (GK) simulations is critical.

In this work, an extensive linear analysis of ETG modes was carried out in NSTX plasmas. Nonlinear simulations to study ETG transport were also performed for particular cases. All the gyrokinetic simulations were local (flux tube) and conducted using the CGYRO code.[20] Four NSTX discharges and one NSTX-U projection were analyzed. Figure 1 shows various profiles of the different analyzed discharges in this work that can affect ETG stability. As can be noted, the profiles cover a wide range in parameter space, which is one of the purposes of this work. NSTX shots 120968 (TRANSP ID 120968A02), 129041 (TRANSP ID 129041A10) and 120982 (TRANSP ID 120982A09) were already employed in ion scale analysis, and they were referred to as high, medium, and low collisionality discharges.[21] The NSTX-U projection, based on NSTX shot 121123 (TRANSP ID 121123K55), was also studied in the same work and referred to an

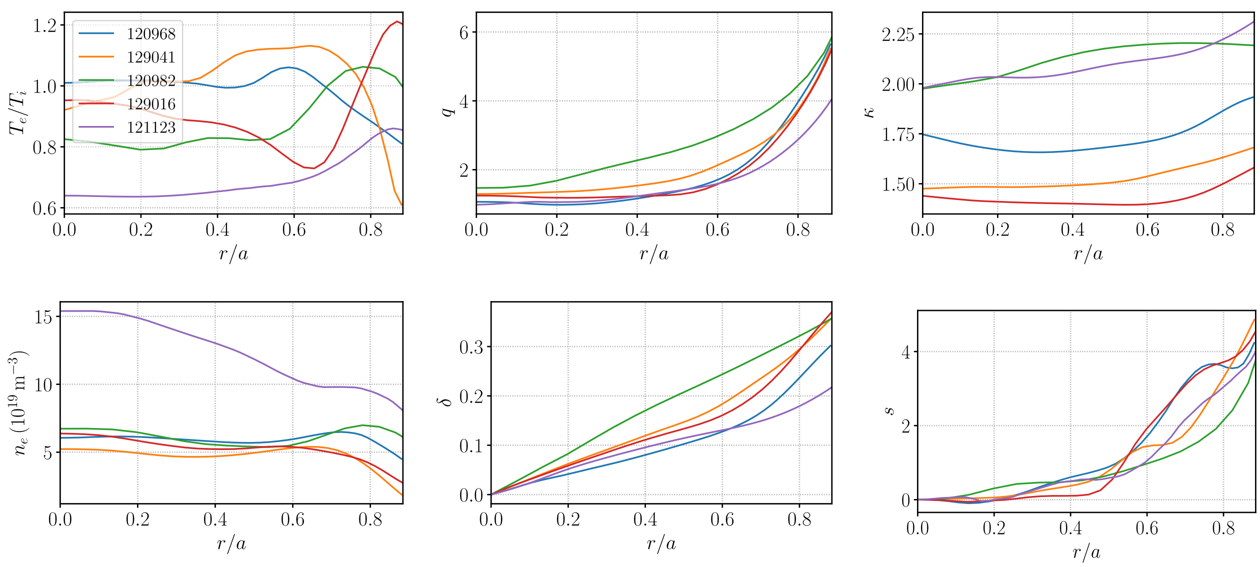

FIG. 1. NSTX profiles for different shots analyzed using linear simulations, displaying the ratio of electron to ion temperatures, T_e/T_i, safety factor, q, elongation, κ, electron density, n_e, magnetic shear, s, and triangularity, δ.

even lower collisionality regime. This is one of the main purposes of NSTX-U, which aims to examine and assess transport in low collisionality regimes.[22,23] Shot 129016 (TRANSP ID 129016A03) was also explored previously, and on which the first ETG gyrokinetic simulations in NSTX were presented.[15] A more complete set of parameters at all the radial locations analyzed in this work can be found in Table I,[24] where standard definition for the various quantities is employed.[20,21] For all the simulations, three kinetic species were included: electrons, deuterons (the main plasma ion species), and carbon as the main impurity. The simulations are constrained to the core region [up to $r/a = 0.8$, where r is the minor radius of the local flux surface, referred here as the radial coordinate, and a the minor radius of the Last-Closed Flux Surface (LCFS)]. The NSTX pedestal region has been separately investigated recently[25–28] and therefore left out of the scope of the present work.

This paper is organized as follows: In Sec. II, a broad set of linear simulations is conducted to determine gyrokinetic ETG thresholds of the different discharges and radial positions described in Table I. An analysis is also conducted to put in evidence different features that ETG may have in high-β and low-aspect-ratio tokamaks. In Sec. III, a nonlinear analysis is presented for one discharge showing convergence tests and scans. In Sec. IV, comparison with reduced models is performed, for both linear and nonlinear calculations, as well as with experimental results obtained from power balance with TRANSP code. Finally, Sec. V presents the conclusions.

II. LINEAR ANALYSIS AND ETG CRITICAL GRADIENTS

As a first step and for each discharge, fully electromagnetic CGYRO[29] linear simulations were conducted over a wide range of wavenumbers to determine the modes present at the nominal experimental conditions. CGYRO uses a combination of spectral and pseudospectral techniques.[20] For these simulations, typical grid resolutions employed were $N_\varepsilon = 8$ (energy), $N_\xi = 16$ (pitch angle) and $N_\theta = 48$ (poloidal). N_{rad}, which defines the number of "connected" flux tubes, was usually chosen to be 6 for electron scale modes and 12 for ion-scale modes, while the number of toroidal modes, N_{tor}, is limited to 1 for linear simulations, and determined by the binormal wavenumber $k_\theta\rho_s$ ($\rho_s = (m_D T_e)^{1/2}/B_{unit}$ is an effective ion-sound gyroradius and B_{unit} is an effective magnetic field.[20] An example of these analysis is presented in Fig. 2. Figure 2 shows the (a) real frequency (in symlog scale) and (b) growth rate for shot 129016 at two radial locations, $r/a = 0.6$ and 0.7, as a function of $k_\theta\rho_s$. From Fig. 2, at $r/a = 0.6$, the dominant mode is indicated as ETG, with other modes present in the ion-scale region, including microtearing modes (MTMs) and kinetic ballooning modes (KBMs), but present with very small growth rates. At $r/a = 0.7$, KBM and MTM are also present. The procedure to identify the ion-scale modes is the same as the one presented in Ref. 21, in which eigenfunctions as well as real frequency and growth rate behavior with different parameters are analyzed to determine the mode nature. However, it is important to note that in both cases, the $E \times B$ flow shearing rate, γ_E, is larger and expected to suppress this ion scale instability [although MTMs could sometimes be unaffected by the flow shear rate as reported in Mega Ampere Spherical Tokamak (MAST) studies[30] or projections to future ST power plants[31]].

In the electron-scale range, it can be seen from Fig. 2(b) that ETG modes peak at $k_\theta\rho_s \approx 20$ ($\rho_s/a = 6.70 \times 10^{-3}$) and 28 ($\rho_s/a = 4.68 \times 10^{-3}$) for $r/a = 0.6$ and 0.7, which corresponds to toroidal mode numbers, $n = k_\theta r/q$, of approximately 1130 and 1800, respectively. The dashed and dotted curves, which are only shown for this range and are almost identical, correspond to simulations with $\delta B_\parallel = 0$ and to electrostatic simulations ($\delta B_\parallel = \delta A_\parallel = 0$), respectively. This comparison is in agreement with the fact that ETG can be usually captured well with electrostatic models. However, as it will be shown below, this is not always the case in spherical tokamaks. To identify the electron scale modes, a similar procedure was employed. Figure 3 shows eigenfunctions of the (a) perturbed electrostatic potential, $\delta\varphi$ (b) perturbed parallel vector potential, $\delta A_\parallel$, and (c) perturbed parallel magnetic field,

TABLE I. Summary of relevant equilibrium parameters at the different radial locations of the analyzed shots.

r/a	R/a	κ	δ	q	s	$\beta_{e,unit}$ (%)	T_e/T_i	a/L_{T_e}	a/L_{n_e}	a/L_{T_i}	a/L_{n_i}	$\alpha_{MHD,unit}$	Z_{eff}	$\nu^{e/i}$ (c_s/a)	γ_E (c_s/a)
(a) Shot #120968 at 560 ms															
0.4	1.58	1.66	0.080	1.16	0.61	5.15	1.00	1.56	0.307	1.40	0.288	0.359	2.06	1.27	0.152
0.6	1.53	1.71	0.127	1.70	1.70	2.51	1.059	2.66	−0.774	2.44	0.686	0.412	2.87	3.91	0.174
0.7	1.50	1.76	0.166	2.47	3.16	1.39	0.980	3.11	−0.469	2.05	−1.37	0.416	2.86	7.54	0.118
0.8	1.46	1.86	0.237	3.97	3.60	0.588	0.885	2.80	2.60	1.92	3.20	1.28	2.77	11.7	0.0883
(b) Shot #129016 at 460 ms															
0.4	1.55	1.40	0.111	1.23	0.104	3.44	0.877	0.982	0.076	0.731	0.022	0.150	1.47	0.778	0.402
0.6	1.51	1.40	0.161	1.58	1.93	1.93	0.752	3.48	0.379	2.47	1.34	0.594	1.68	1.91	0.757
0.7	1.47	1.43	0.211	2.32	3.09	0.869	0.787	3.28	1.10	6.00	1.35	0.839	1.95	4.24	0.408
0.8	1.44	1.50	0.293	3.69	3.71	0.357	1.087	2.07	3.33	4.79	6.29	0.882	2.50	7.12	0.060
(c) Shot #129041 at 490 ms															
0.4	1.55	1.49	0.119	1.54	0.37	3.77	1.063	0.37	−0.299	1.19	0.47	0.129	3.23	0.71	0.144
0.6	1.51	1.54	0.184	2.13	1.45	2.65	1.126	1.44	−0.545	1.57	1.22	0.392	3.33	1.07	0.163
0.7	1.49	1.58	0.235	2.70	1.78	1.70	1.110	2.07	1.21	1.39	5.19	1.02	4.07	1.80	0.132
0.8	1.45	1.63	0.295	3.75	3.30	0.626	0.943	4.95	5.75	1.55	6.72	1.76	4.75	2.78	0.138
(d) Shot #120982 at 620 ms															
0.4	1.66	2.15	0.170	2.27	0.488	1.90	0.833	0.453	0.398	0.47	0.439	0.300	1.55	0.355	0.119
0.6	1.60	2.20	0.244	2.97	0.972	1.17	0.869	1.59	−0.931	2.86	−0.0948	0.543	1.78	0.578	0.297
0.7	1.56	2.20	0.282	3.55	1.36	0.933	1.017	2.19	−1.53	3.34	−0.598	0.486	2.23	1.22	0.211
0.8	1.52	2.20	0.321	4.43	2.11	0.627	1.063	3.01	0.348	3.00	0.972	1.15	2.41	2.28	0.0932
(e) NSTX-U projection #121123 at 14500 ms															
0.4	1.94	2.06	0.0956	1.23	0.50	3.68	0.653	0.454	0.75	0.66	0.75	0.325	2.0	0.178	0.048
0.6	1.89	2.12	0.131	1.59	1.05	1.88	0.685	2.04	1.22	2.45	1.22	0.695	2.0	0.219	0.129
0.7	1.85	2.15	0.149	2.03	2.17	1.09	0.735	3.04	−0.0446	3.99	−0.0446	0.623	2.0	0.339	0.0984
0.8	1.81	2.22	0.179	2.87	3.05	0.544	0.826	3.82	0.973	5.02	0.973	0.883	2.0	0.621	0.0183

$\delta B_\parallel$, for the mode with $k_\theta \rho_s = 20$ at $r/a = 0.6$ (all the linear analysis in this section was conducted with $\theta_0 = 0$, assuming this is the most unstable ETG mode). Eigenfunctions show twisting (or ballooning) parity, which is a feature of ETG modes. In addition, Figs. 3(d) and 3(e) present a scan over the electron temperature gradient scale length (we will refer this just as the temperature gradient), a/L_{T_e}, for selected wavenumbers, showing the sensitivity of the growth rate to this parameter. These scans were conducted keeping the equilibrium pressure gradient β' (i.e., $\alpha_{MHD,unit}$) fixed. Therefore, the local equilibrium remained unchanged.

The scans presented in Figs. 3(c) and 3(d) also serve to estimate the linear ETG threshold or critical gradient, defined as the minimum a/L_{T_e} value at which ETG growth rate arises for any wavenumber. Since it is usually numerically challenging to scan to very small growth rates, a simple linear extrapolation is employed to determine the actual ETG threshold, as indicated with the dashed lines.

A similar procedure as the one described for Fig. 3 was conducted for all the different discharges indicated in Table I, in which the ETG threshold was determined for the radial region $r/a = 0.4$–0.8. The results for each discharge are presented in Fig. 4, which shows the experimental temperature gradient, $(R/L_{T_e})^{(\mathrm{exp})}$, along with the ETG critical gradient (or threshold) inferred from the linear gyrokinetic simulations, $(R/L_{T_e})^{(GK)}_{ETG}$. By comparing the inferred threshold from GK simulations with the experimental value, it is clear that ETG modes are present in several cases while suppressed in others.

Figure 4 also includes a simple scaling expression, $(R/L_{T_e})^{(J)}_{ETG} = \max\{(1 + Z_{eff} T_e/T_i)(1.33 + 1.91 s/q)(1 - 1.5\varepsilon)(1 + 0.3 r d\kappa/dr), 0.8 R L_{n_e}\}$, derived for conventional aspect ratio tokamaks.[32] It can be observed that the $(R/L_{T_e})^{(J)}_{ETG}$ expression is not in good agreement with $(R/L_{T_e})^{(GK)}_{ETG}$, which exposes the limitation of this formula when applied to low aspect ratio spherical tokamaks. It is important to clarify that the development of this formula was not intended for these conditions, but it has been used as a proxy in previous studies.[12,15,33]

To put in evidence the complex physics that impacts the scaling properties of ETG thresholds in spherical tokamaks, scans over magnetic shear, s, elongation, κ, and safety factor, q, were conducted

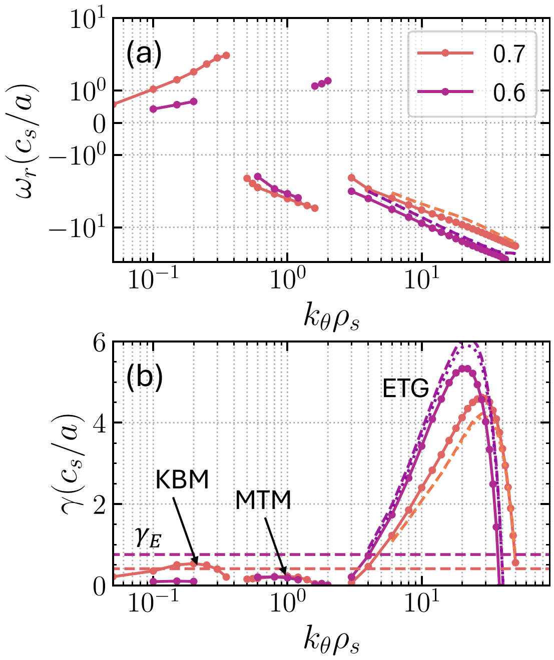

FIG. 2. (a) Real frequency, ω_r, and (b) growth rate, γ of shot 129016 as a function of the wavenumber, $k_\theta \rho_s$, for two radial locations, $r/a = 0.6$ and 0.7. Different modes are present. Dashed and dotted curves show ETG results with $\delta B_\parallel = 0$ and $\delta B_\parallel = \delta A_\parallel = 0$, respectively.

around the equilibrium value of different discharges (these scans were conducted keeping $\beta^* = -(8\pi/B_{unit}^2)dp/dr$ fixed). Figure 5 shows the results for shots 129016 and 120982 at $r/a = 0.6$ and $r/a = 0.8$, respectively. It can be noted that very different behavior arises in both cases: ETG threshold increases with magnetic shear for shot 129016 as

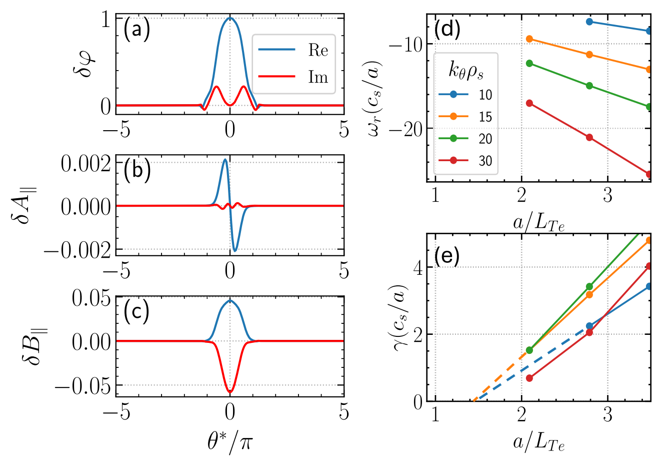

FIG. 3. Eigenfunctions of the (a) perturbed electrostatic potential, (b) the perturbed parallel vector potential, and (c) the parallel magnetic field, corresponding to a mode with $k_\theta \rho_s = 20$ (shot 129016 at $r/a = 0.6$). (d) Real frequency and (e) growth rates of modes at the same radial location, scanned over the electron temperature gradient to determine the ETG growth rate threshold.

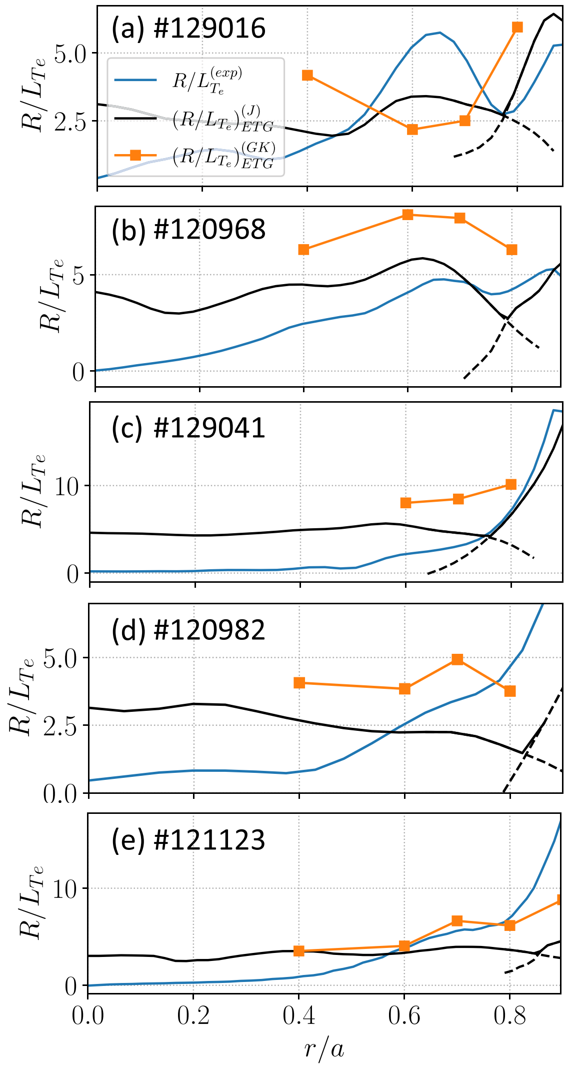

FIG. 4. ETG threshold (or critical gradient) profiles inferred from CGYRO linear simulations, $(R/L_{T_e})_{ETG}^{(GK)}$, for the different analyzed discharges. The experimental nominal profile, $(R/L_{T_e})^{(exp)}$, and an explicit expression derived for conventional aspect ratio tokamaks, $(R/L_{T_e})_{ETG}^{(J)}$, are included for reference.

it does for standard tokamaks (as inferred from the $(R/L_{T_e})_{ETG}^{(J)}$ formula). However, the opposite trend occurs for shot 120982. When scaling over elongation, both cases show a threshold from which the ETG threshold starts to increase and become sensitive to the plasma elongation. Finally, the scan over the safety factor also reveals opposite trends: the ETG threshold decreases as the safety factor increases for shot 129016, similarly to conventional tokamaks, but for shot 120982, the ETG threshold shows a critical value after which it increases. It is important to note that similar findings were already pointed out by Patel *et al.*[31] in which ETG critical gradients were explored in expected regimes of a high-β spherical tokamak fusion reactor, therefore confirming this different behavior.

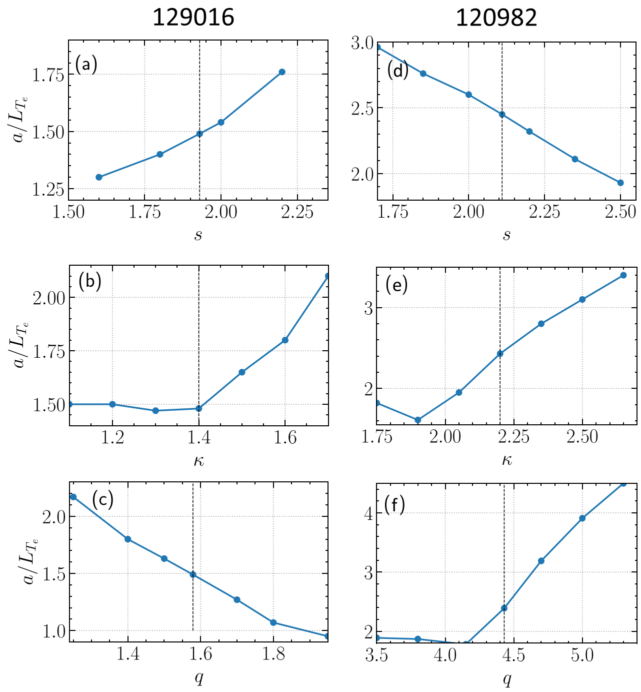

FIG. 5. ETG threshold inferred from linear CGYRO simulations for shot 129016 at $r/a = 0.6$ (a)–(c) and shot 120982 at $r/a = 0.8$ (d)–(f) as a function of the magnetic shear, s, elongation, κ, and safety factor, q. The trend observed in the first case agrees with standard ETG threshold while in the second case, different trends are observed.

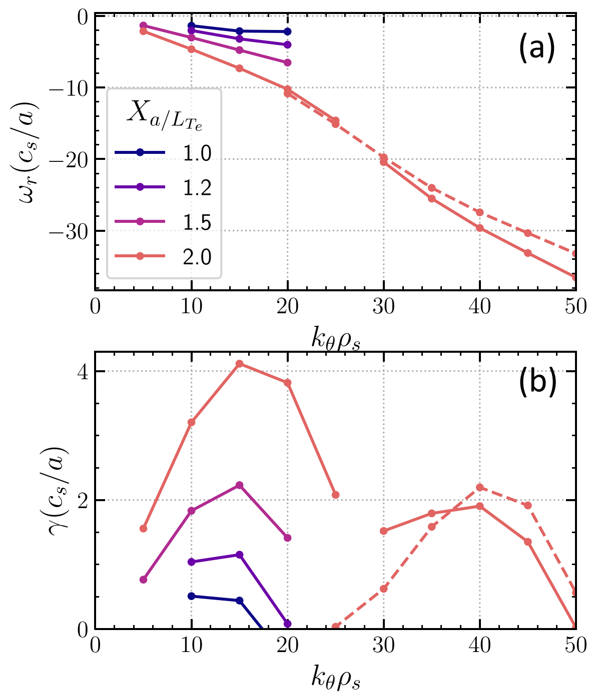

FIG. 6. (a) Real frequency and (b) growth rates over a wide range of wavenumbers $k_\theta \rho_s$, corresponding to shot 120982 at $r/a = 0.8$, and scaling over the electron temperature gradient (indicated as a scaling factor, $X_{a/L_{T_e}}$). The dash curve is the result when $\delta B_\parallel$ is turned off in the model.

The different ETG threshold behavior in shots 120982 and 129016 could be due to a number of reasons, like the large difference in safety factor, among others and should be further explored in future studies. Here, an additional analysis is presented in Fig. 6, showing (a) real frequencies and (b) growth rates over a wide range of wavenumbers, and for different electron temperature gradients, indicated with the scaling factor, $X_{a/L_{T_e}}$ (where "1.0" means the experimental value of $a/L_{T_e} = 3.01$). As with the scans shown in Fig. 3, these scans were conducted keeping β' fixed.

It can be seen that growth rates peaking at $k_\theta \rho_s \sim 10$–15 are very sensitive to the electron temperature gradient, which is consistent with ETG modes. Another peak arises at $k_\theta \rho_s \sim 40$ after doubling the experimental nominal value of the electron temperature gradient. The dash curve shows results when $\delta B_\parallel$ is turned off. Interestingly, the first peak vanishes when the parallel magnetic field perturbation is not included, while the second peak is more resilient, as it is the usual case of ETG modes. Although not shown here, all these modes present twisting or ballooning parity, and the quasilinear flux shows that the electron thermal flux, Q_e, is dominated by the electrostatic potential $\delta\varphi$, as expected for ETG modes. We therefore conclude that all the modes present in Fig. 6 are ETG modes, but the first branch (meaning the modes peaking at $k_\theta \rho_s \sim 10$–15) requires a full electromagnetic model to drive those modes unstable. The effect of the compressional magnetic field, $\delta B_\parallel$, was already pointed out to be important to be included in gyrokinetic simulations for in high-β spherical tokamaks.[34] A recently study also showed the importance of the compressional magnetic field in the context of hybrid KBMs in the Spherical Tokamak for Energy Production (STEP).[35] Because of this, a simple formula like the ones used for conventional tokamaks might not be enough to describe ETG critical gradients in these conditions. Scaling laws for ETG threshold in spherical tokamaks should consider additional effects that arise in these regimes.

To summarize this section, Fig. 7 shows the ETG critical gradient threshold as a function of the corresponding experimental temperature

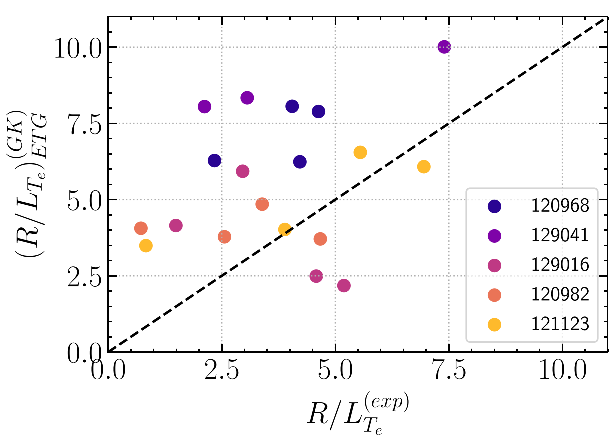

FIG. 7. ETG critical temperature gradient thresholds from CGYRO linear analysis against their corresponding experimental value, combining all the analyzed discharges and radial positions.

gradient, combining all the analyzed discharges and radial positions. The dashed curve indicates the condition when the ETG threshold is at the experimental value of the temperature gradient. A similar summary was presented in Ref. 21 which clearly showed a correlation of experimental profiles with KBM threshold, while Ion Temperature Gradient (ITG) thresholds were shown to be mostly above the corresponding experimental value. Here, Fig. 7 does not show a clear correlation suggesting that the ETG may not always impose a stiff limit, and therefore the critical gradient cannot be directly used to determine the electron temperature profile.

III. NONLINEAR ANALYSIS

In this section, nonlinear gyrokinetic simulations were conducted to assess the thermal transport caused by ETG modes. In particular, the analysis presented in this section is performed for shot 129016 and at $r/a = 0.6$, for which linear simulations were discussed in the previous section. The next section will use the results presented here and include results at $r/a = 0.7$ in order to compare them with reduced models as well as the experiment. These cases were chosen because the linear analysis showed no ion-scale modes with growth rates larger than the corresponding $E \times B$ shearing rate. With this criteria, and in order to simplify the computation, it is assumed that there is no ion-scale contribution to the electron thermal flux, and therefore, it is important to note that the simulations were not multi-scale in the sense that ion-scale modes were not included but limited to the electron scale. As a first step, a convergence analysis was performed where radial (N_{rad}) and binormal (N_{tor}) grid resolution were changed. Table II shows an example of the different values chosen as well as other related quantities employed in the simulations.

Figure 8(a) shows the electron thermal flux evolution during the simulations, which clearly saturates for all cases described in Table II. The horizontal dashed lines represent average values that are shown for reference. In addition, Fig. 8(b) shows the electron thermal flux spectra during the saturated phase. It can be observed that the turbulent cascade is well covered, with a peak around $k_\theta \rho_s \sim 9$–10, in agreement with the linear case.

To assess the effect of the flow shearing rate, and to account for uncertainties in the nominal value of the electron temperature gradients, nonlinear simulations were performed varying both quantities (keeping the equilibrium pressure gradient fixed, as in the linear simulations presented in the previous section). This is shown in Fig. 9, where thermal flux spectra are presented for different values of (a) γ_E and (b) a/L_{T_e}. The total flux obtained in each case is $6.3 \pm 0.3\,(1\gamma_E)$, $5.8 \pm 0.2\,(1.2\gamma_E)$, $4.2 \pm 0.3\,(1.5\gamma_E)$, $2.6 \pm 0.2\,(2\gamma_E)$ and $1.8 \pm 0.2\,(0.8a/L_{T_e})$, $6.3 \pm 0.3\,(1a/L_{T_e})$, $15.5 \pm 0.3\,(1.2a/L_{T_e})$. The $E \times B$ flow shear rate has a stronger impact on low-$k_\theta \rho_s$, as expected, while increasing the electron temperature gradients impacts the entire spectrum since a broader range of modes becomes unstable.

TABLE II. Different CGYRO resolutions employed to test convergence. The remaining grid resolution values were: $n_\theta = 48$, $n_\xi = 16$, and $n_\varepsilon = 8$.

Case	N_{rad}	N_{tor}	$\Delta k_x \rho_s$	$\Delta k_\theta \rho_s$	L_x/ρ_s	L_y/ρ_s
A	96	26	1.82	3	3.5	2.1
B	144	26	1.01	3	6.2	2.1
C	144	34	1.03	2.2	6.1	2.9

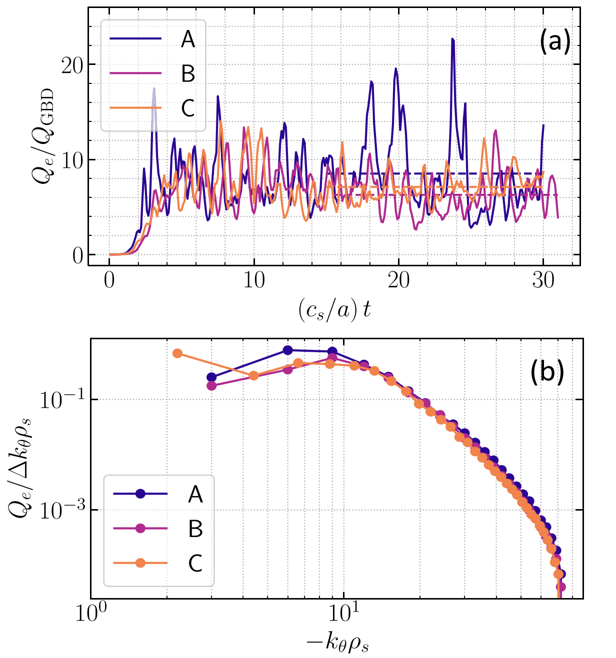

FIG. 8. Convergence test for shot 129016 at $r/a = 0.6$: (a) Total electron thermal flux evolution showing saturation for three different grid resolutions indicated in Table II. (b) Electron thermal flux spectra averaging over the time window indicated with the dashed lines in (a).

IV. POWER FLOW AND COMPARISON WITH REDUCED MODELS

In this section, linear and nonlinear CGYRO results are compared with reduced models and with values inferred from the experiments. Figure 10 shows real frequency and growth rate of the shot 129016 presented in Fig. 2 at (a) and (b) $r/a = 0.6$ and (c) and (d) $r/a = 0.7$, but compared with a reduced model developed for ETG modes, ETGM (which is part of the multi-mode model, or MMM),[36,37] as well as Trapped-Gyro-Landau-Fluid (TGLF),[38,39] which has been widely used in conventional tokamaks. Both reduced models find unstable ETG modes at this condition, in agreement with CGYRO. Here, the electrostatic (ES) model of TGLF is employed, but the electromagnetic model gives a similar linear result. Real frequencies at $r/a = 0.6$ are well reproduced by both reduced models. TGLF also reproduces the real frequency at $r/a = 0.7$ in good agreement with CGYRO, whereas ETGM shows a deviation. When looking at the growth rates, some noticeable discrepancies arise. ETGM growth rate presents a similar behavior to CGYRO matching the maximum growth rate value, although the overall trend is shifted toward lower wavenumbers. This difference may stem from the method used to incorporate finite Larmor radius (FLR) effects in the ETGM model, which relies on the norm of $\langle k_\perp \rangle$ derived from a well-localized eigenfunction. To address this discrepancy, the ETGM model's thermal diffusivity was calibrated using NSTX discharges.[36] Once calibrated, the model maintains consistency without adjustments across different discharges.[40] TGLF also presents growth rates trends similar to CGYRO but they are systematically overpredicted and not showing a maximum

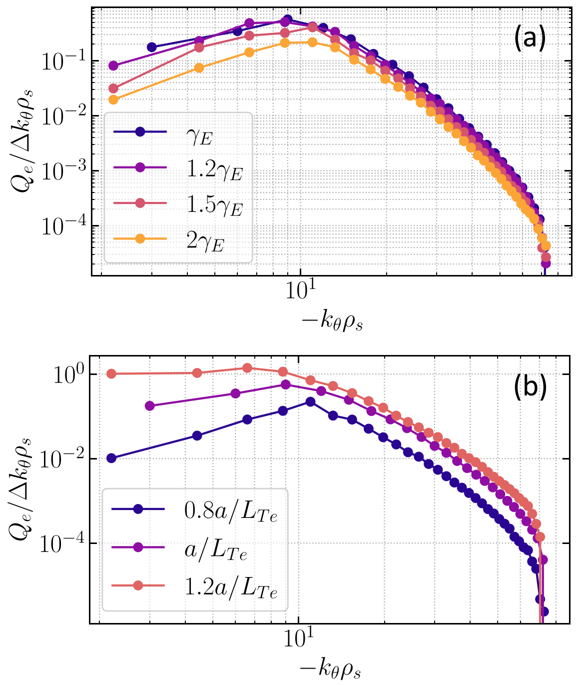

FIG. 9. ETG electron thermal flux spectra for (a) different $E \times B$ flow shearing rates ($\gamma_E = 0.757 c_s/a$), and for (b) different values of the electron temperature gradient ($a/L_{T_e} = 3.48$). Lower $k_\theta \rho_s$ modes are affected by γ_E, while a/L_{T_e} affects the entire spectra.

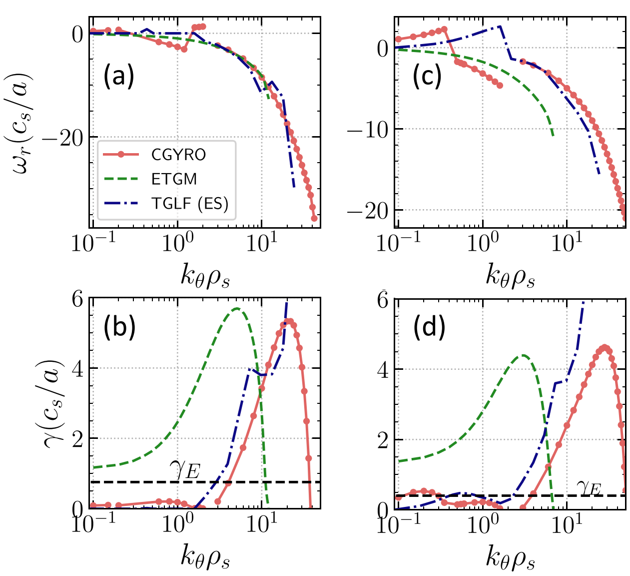

FIG. 10. Comparison of CGYRO linear simulations with reduced models ETGM and TGLF for shot 129016 at (a) and (b) $r/a = 0.6$ and (c) and (d) $r/a = 0.7$.

within the analyzed range of wavenumbers. This overprediction of TGLF was already pointed out in a recent study.[41] As it will be shown below, this does not necessarily reflect on higher fluxes, as they are certainly dependent on the employed saturation rule. In addition, even it is not shown here, both TGLF and ETGM do not show a clear ETG threshold as CGYRO does. When substantially reducing a/L_{T_e} at $r/a = 0.6$ in both reduced models, there was always a nonzero growth rate for at least one wavenumber.

Nonetheless, the main purpose of these reduced models is to use them for profile prediction and even for real-time plasma control. This is related to the thermal energy flux and, therefore, with CGYRO nonlinear calculations. The nonlinear simulations presented in the previous Sec. allow the calculation of the total power flow. This is presented in Fig. 11, which shows the total power flow through the (a) $r/a = 0.6$ and (b) 0.7 flux surfaces for the shot 129016. The experimental value is marked with a black star, and a 20% error bar is assumed, which is consistent with uncertainties employed previously.[15,17] From the linear analysis presented in Fig. 2, it is reasonable to expect that, for $r/a = 0.6$, all the transport is caused by ETGs, while at $r/a = 0.7$, either KBMs or MTMs can potentially play a role since they are near threshold. CGYRO results are shown with circles and for three flow shear rates in both cases (at $r/a = 0.6$, $\gamma_E = 0.757\, c_s/a$, and at

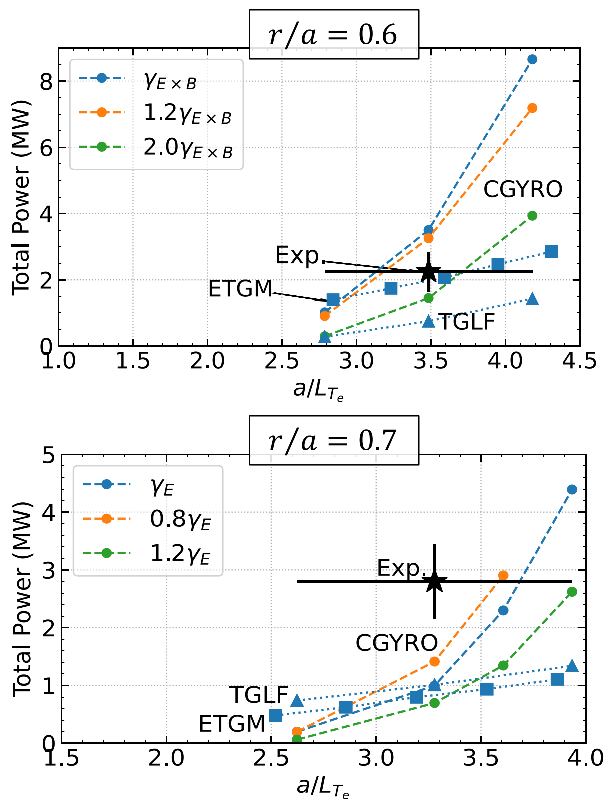

FIG. 11. Power flow through the flux surface $r/a = 0.6$ (top) and $r/a = 0.7$ (bottom) for shot 129016 at 460 ms. Experimental value is indicated with a black star with a 20% generic error bar assumed. CGYRO results are indicated with circles and colors refer to different values of the flow shearing rate, γ_E. Results from ETGM and TGLF are included in squares and triangles, respectively.

$r/a = 0.7$, $\gamma_E = 0.403\, c_s/a$). Simulations are also presented as a function of the electron temperature gradient, scanning over different values, to account for experimental uncertainties. It can be observed that the comparisons with NSTX experimental data are in agreement within the uncertainties.

In addition, Fig. 11 shows results from the reduced model ETGM in squares.[42] As mentioned before, ETGM was calibrated to NSTX data, but it is worth noting again that the calibration is global and not constrained to a particular flux surface. Therefore, although the $r/a = 0.6$ surface lies within the global plasma conditions used for ETGM calibration, the agreement between ETGM results and the experimental nominal value at $r/a = 0.6$ for this particular discharge, as well as with the CGYRO simulations, is significant. This provides confidence on the use of ETGM for profile prediction in future NSTX-U discharges, but further analysis would still be valuable. The results of the reduced model TGLF (indicated with triangles) are also included for comparison, which properly identify the presence of ETG modes. For these cases, the TGLF SAT0 rule was employed and was found to perform better than the newer SAT1 or SAT2 rules, which presented a much stronger sensitivity on the electron temperature gradient and substantially over-predicted the power flow in some cases (not shown here). These newer saturation rules account for multiscale effects and might be the cause of discrepancy, as mentioned in Ref. 41, and further investigation is still necessary. The values obtained by TGLF SAT0 show that it underpredicts the power flow at $r/a = 0.6$. At $r/a = 0.7$, the power flow matches CGYRO nominal value. However, for this radial position, a significant fraction of the electron thermal flux ($\sim$60% at the nominal a/L_{T_e} value) comes from low-$k_\theta \rho_s$ range, corresponding to ion-scale modes observed in the linear simulations. As an additional test, electron thermal flux from reduced models were calculated at $r/a = 0.8$, in which CGYRO linear analysis showed that ETG is stable at the experimental nominal value [see Fig. 4(a)]. Although not shown here, at this radial location both ETGM and TGLF SAT0 predict negligible electro-scale transport, as expected.

Finally, it is important to note that the scaling of the power flow with the electron temperature gradient differs between CGYRO and the reduced models. Both ETGM and TGLF exhibit similar linear scaling behavior, in contrast to CGYRO, which displays for these cases a power-law-like trend, which corresponds to a stiff transport. This discrepancy also warrants further investigation and understanding.

V. CONCLUSIONS

Extensive linear gyrokinetic simulations were conducted on several NSTX discharges and on an NSTX-U projection to analyze the occurrence and thresholds of ETG modes. The discharges covered a wide range of parameter space. ETG threshold profiles were determined, finding that the modes are usually present in some discharges while suppressed in others at the experimental value. The ETG threshold in spherical tokamaks is shown to follow a more complex physics and a simple analytic formula might not be possible since different trends are observed in different cases. Non-linear simulations were also conducted for a particular discharge, showing that CGYRO results are consistent with the transport levels expected in the experiments. In addition, a comparison of gyrokinetic simulations with reduced models ETGM and TGLF, critical for fast profile prediction, was also conducted. Both ETGM and TGLF models captured ETG physics. On one side, the ETGM model has shown power flow close to experimental values, as have the CGYRO nonlinear simulations. Conversely, TGLF-SAT0 underpredicted the power flow coming from ETG modes. In addition, there are discrepancies of both reduced models compared to CGYRO, such us the lack of rollover in the TGLF growth rate, the shift of the frequency and/or growth rate in ETGM, and the lack of a well-defined threshold inferred from the linear simulations in both cases. Finally, the scaling of the power flow with the electron temperature gradient shows differences between CGYRO, which shows a power-like trend corresponding to a stiff transport, and ETGM and TGLF reduced models, which show a more linear-like trend. Therefore, further comparisons would be valuable to continue understanding their applicability and limitations.

ACKNOWLEDGMENTS

This work was supported by the U.S. Department of Energy, Office of Science, under Award Numbers DE-SC0021385, DE-SC0013977, DE-SC0021113, and DE-AC02-09CH11466. This research used resources of the National Energy Research Scientific Computing Center (NERSC), a Department of Energy Office of Science User Facility. The authors acknowledge NSTX-U scientists, who helped make the experimental profile measurements.

AUTHOR DECLARATIONS

Conflict of Interest

The authors have no conflicts to disclose.

Author Contributions

C. F. Clauser: Formal analysis (lead); Investigation (lead); Methodology (equal); Writing – original draft (lead). **T. Rafiq:** Investigation (equal); Methodology (equal); Supervision (equal); Writing – review & editing (equal). **J. Parisi:** Investigation (equal); Methodology (equal); Writing – review & editing (equal). **G. Avdeeva:** Formal analysis (equal); Investigation (equal); Writing – review & editing (equal). **W. Guttenfelder:** Investigation (equal); Methodology (equal); Supervision (equal); Writing – review & editing (equal). **E. Schuster:** Project administration (equal); Supervision (equal). **C. Wilson:** Investigation (equal).

DATA AVAILABILITY

The data that support the findings of this paper is available in Princeton Data Commons.[43]

REFERENCES

1. S. M. Kaye, R. E. Bell, D. Gates, B. P. LeBlanc, F. M. Levinton, J. E. Menard, D. Mueller, G. Rewoldt, S. A. Sabbagh, W. Wang, and H. Yuh, "Scaling of electron and ion transport in the high-power spherical torus NSTX," Phys. Rev. Lett. **98**, 175002 (2007).
2. S. Kaye, F. Levinton, D. Stutman, K. Tritz, H. Yuh, M. Bell, R. Bell, C. Domier, D. Gates, W. Horton, J. Kim, B. LeBlanc, N. Luhmann, R. Maingi, E. Mazzucato, J. Menard, D. Mikkelsen, D. Mueller, H. Park, G. Rewoldt, S. Sabbagh, D. Smith, and W. Wang, "Confinement and local transport in the National Spherical Torus Experiment (NSTX)," Nucl. Fusion **47**, 499–509 (2007).
3. W. Dorland, F. Jenko, M. Kotschenreuther, and B. N. Rogers, "Electron temperature gradient turbulence," Phys. Rev. Lett. **85**, 5579–5582 (2000).
4. F. Jenko, W. Dorland, M. Kotschenreuther, and B. N. Rogers, "Electron temperature gradient driven turbulence," Phys. Plasmas **7**, 1904–1910 (2000).

[5]Y. Ren, W. Guttenfelder, S. M. Kaye, and W. X. Wang, "Transport from electron-scale turbulence in toroidal magnetic confinement devices," Rev. Mod. Plasma Phys. **8**, 5 (2024).
[6]W. Guttenfelder, R. Groebner, J. Canik, B. Grierson, E. Belli, and J. Candy, "Testing predictions of electron scale turbulent pedestal transport in two DIII-D ELMy H-modes," Nucl. Fusion **61**, 056005 (2021).
[7]B. Chapman-Oplopoiou, D. Hatch, A. Field, L. Frassinetti, J. Hillesheim, L. Horvath, C. Maggi, J. Parisi, C. Roach, S. Saarelma, J. Walker, and J. Contributors, "The role of ETG modes in JET–ILW pedestals with varying levels of power and fuelling," Nucl. Fusion **62**, 086028 (2022).
[8]J. F. Parisi, F. I. Parra, C. M. Roach, C. Giroud, W. Dorland, D. R. Hatch, M. Barnes, J. C. Hillesheim, N. Aiba, J. Ball, P. G. Ivanov, and JET Contributors, "Toroidal and slab ETG instability dominance in the linear spectrum of JET-ILW pedestals," Nucl. Fusion **60**, 126045 (2020).
[9]A. R. Field, B. Chapman-Oplopoiou, J. W. Connor, L. Frassinetti, D. R. Hatch, C. M. Roach, S. Saarelma, and J. Contributors, "Comparing pedestal structure in JET-ILW H-mode plasmas with a model for stiff ETG turbulent heat transport," Philos. Trans. R. Soc. A **381**, 20210228 (2023).
[10]C. M. Roach, I. G. Abel, R. J. Akers, W. Arter, M. Barnes, Y. Camenen, F. J. Casson, G. Colyer, J. W. Connor, S. C. Cowley, D. Dickinson, W. Dorland, A. R. Field, W. Guttenfelder, G. W. Hammett, R. J. Hastie, E. Highcock, N. F. Loureiro, A. G. Peeters, M. Reshko, S. Saarelma, A. A. Schekochihin, M. Valovic, and H. R. Wilson, "Gyrokinetic simulations of spherical tokamaks," Plasma Phys. Controlled Fusion **51**, 124020 (2009).
[11]S. M. Kaye, J. W. Connor, and C. M. Roach, "Thermal confinement and transport in spherical tokamaks: A review," Plasma Phys. Controlled Fusion **63**, 123001 (2021).
[12]E. Mazzucato, D. R. Smith, R. E. Bell, S. M. Kaye, J. C. Hosea, B. P. LeBlanc, J. R. Wilson, P. M. Ryan, C. W. Domier, N. C. Luhmann, H. Yuh, W. Lee, and H. Park, "Short-scale turbulent fluctuations driven by the electron-temperature gradient in the national spherical torus experiment," Phys. Rev. Lett. **101**, 075001 (2008).
[13]D. R. Smith, S. M. Kaye, W. Lee, E. Mazzucato, H. K. Park, R. E. Bell, C. W. Domier, B. P. LeBlanc, F. M. Levinton, N. C. Luhmann, J. E. Menard, and H. Yuh, "Electron gyroscale fluctuation measurements in National Spherical Torus Experiment H-mode plasmas," Phys. Plasmas **16**, 112507 (2009).
[14]Y. Ren, W. Guttenfelder, S. M. Kaye, E. Mazzucato, R. E. Bell, A. Diallo, C. W. Domier, B. P. LeBlanc, K. C. Lee, D. R. Smith, and H. Yuh, "Experimental study of parametric dependence of electron-scale turbulence in a spherical tokamak," Phys. Plasmas **19**, 056125 (2012).
[15]W. Guttenfelder, J. Peterson, J. Candy, S. Kaye, Y. Ren, R. Bell, G. Hammett, B. LeBlanc, D. Mikkelsen, W. Nevins, and H. Yuh, "Progress in simulating turbulent electron thermal transport in NSTX," Nucl. Fusion **53**, 093022 (2013).
[16]Y. Ren, E. Belova, N. Gorelenkov, W. Guttenfelder, S. Kaye, E. Mazzucato, J. Peterson, D. Smith, D. Stutman, K. Tritz, W. Wang, H. Yuh, R. Bell, C. Domier, and B. LeBlanc, "Recent progress in understanding electron thermal transport in NSTX," Nucl. Fusion **57**, 072002 (2017).
[17]J. R. Ruiz, W. Guttenfelder, A. E. White, N. T. Howard, J. Candy, Y. Ren, D. R. Smith, N. F. Loureiro, C. Holland, and C. W. Domier, "Validation of gyrokinetic simulations of a National Spherical Torus eXperiment H-mode plasma and comparisons with a high-k scattering synthetic diagnostic," Plasma Phys. Controlled Fusion **61**, 115015 (2019).
[18]S. Kaye, D. Battaglia, D. Baver, E. Belova, J. Berkery, V. Duarte, N. Ferraro, E. Fredrickson, N. Gorelenkov, W. Guttenfelder, G. Hao, W. Heidbrink, O. Izacard, D. Kim, I. Krebs, R. L. Haye, J. Lestz, D. Liu, L. Morton, J. Myra, D. Pfefferle, M. Podesta, Y. Ren, J. Riquezes, S. Sabbagh, M. Schneller, F. Scotti, V. Soukhanovskii, S. Zweben, J. Ahn, J. Allain, R. Barchfeld, F. Bedoya, R. Bell, N. Bertelli, A. Bhattacharjee, M. Boyer, D. Brennan, G. Canal, J. Canik, N. Crocker, D. Darrow, L. Delgado-Aparicio, A. Diallo, C. Domier, F. Ebrahimi, T. Evans, R. Fonck, H. Frerichs, K. Gan, S. Gerhardt, T. Gray, T. Jarboe, S. Jardin, M. Jaworski, R. Kaita, B. Koel, E. Kolemen, D. Kriete, S. Kubota, B. LeBlanc, F. Levinton, N. Luhmann, R. Lunsford, R. Maingi, R. Maqueda, J. Menard, D. Mueller, C. Myers, M. Ono, J.-K. Park, R. Perkins, F. Poli, R. Raman, M. Reinke, T. Rhodes, C. Rowley, D. Russell, E. Schuster, O. Schmitz, Y. Sechrest, C. Skinner, D. Smith, T. Stotzfus-Dueck, B. Stratton, G. Taylor, K. Tritz, W. Wang, Z. Wang, I. Waters, and B. Wirth, "NSTX/NSTX-U theory, modeling and analysis results," Nucl. Fusion **59**, 112007 (2019).
[19]W. Guttenfelder and J. Candy, "Resolving electron scale turbulence in spherical tokamaks with flow shear," Phys. Plasmas **18**, 022506 (2011).
[20]J. Candy, E. Belli, and R. Bravenec, "A high-accuracy Eulerian gyrokinetic solver for collisional plasmas," J. Comput. Phys. **324**, 73–93 (2016).
[21]C. F. Clauser, W. Guttenfelder, T. Rafiq, and E. Schuster, "Linear ion-scale microstability analysis of high and low-collisionality NSTX discharges and NSTX-U projections," Phys. Plasmas **29**, 102303 (2022).
[22]W. Guttenfelder, D. Battaglia, E. Belova, N. Bertelli, M. Boyer, C. Chang, A. Diallo, V. Duarte, F. Ebrahimi, E. Emdee, N. Ferraro, E. Fredrickson, N. Gorelenkov, W. Heidbrink, Z. Ilhan, S. Kaye, E.-H. Kim, A. Kleiner, F. Laggner, M. Lampert, J. Lestz, C. Liu, D. Liu, T. Looby, N. Mandell, R. Maingi, J. Myra, S. Munaretto, M. Podestà, T. Rafiq, R. Raman, M. Reinke, Y. Ren, J. R. Ruiz, F. Scotti, S. Shiraiwa, V. Soukhanovskii, P. Vail, Z. Wang, W. Wehner, A. White, R. White, B. Woods, J. Yang, S. Zweben, S. Banerjee, R. Barchfeld, R. Bell, J. Berkery, A. Bhattacharjee, A. Bierwage, G. Canal, X. Chen, C. Clauser, N. Crocker, C. Domier, T. Evans, M. Francisquez, K. Gan, S. Gerhardt, R. Goldston, T. Gray, A. Hakim, G. Hammett, S. Jardin, R. Kaita, B. Koel, E. Kolemen, S.-H. Ku, S. Kubota, B. LeBlanc, F. Levinton, J. Lore, N. Luhmann, R. Lunsford, R. Maqueda, J. Menard, J. Nichols, M. Ono, J.-K. Park, F. Poli, T. Rhodes, J. Riquezes, D. Russell, S. Sabbagh, E. Schuster, D. Smith, D. Stotler, B. Stratton, K. Tritz, W. Wang, and B. Wirth, "NSTX-U theory, modeling and analysis results," Nucl. Fusion **62**, 042023 (2022).
[23]J. W. Berkery, P. O. Adebayo-Ige, H. Al Khawaldeh, G. Avdeeva, S. G. Baek, S. Banerjee, K. Barada, D. Battaglia, R. E. Bell, E. A. Belli, E. Belova, N. Bertelli, N. Bisai, P. T. Bonoli, D. Boyer, J. Butt, J. Candy, C. S. Chang, C. F. Clauser, L. Corona Rivera, M. Curie, P. C. de Vries, R. Diab, A. Diallo, J. Dominski, V. N. Duarte, E. Emdee, N. Ferraro, R. Fitzpatrick, E. L. Foley, E. Fredrickson, M. Galante, K. Gan, S. P. Gerhardt, R. J. Goldston, W. Guttenfelder, R. Hager, M. O. Hanson, S. C. Jardin, T. G. Jenkins, S. M. Kaye, A. Khodak, J. Kinsey, A. Kleiner, E. Kolemen, S.-H. Ku, M. Lampert, B. Leard, B. P. LeBlanc, J. Lestz, F. Levinton, C. Liu, T. Looby, R. Lunsford, T. Macwan, R. Maingi, J. McClenaghan, J. E. Menard, S. Munaretto, M. Ono, A. Pajares, J. F. Parisi, J.-K. Park, M. Parsons, B. S. Patel, Y. V. Petrov, M. Podesta, F. Poli, M. Porcelli, T. Rafiq, S. A. Sabbagh, A. Sanchez-Villar, E. Schuster, J. Schwartz, A. Sharma, S. Shiraiwa, P. Sinha, D. Smith, S. P. Smith, V. Soukhanovskii, G. M. Staebler, E. A. Startsev, B. Stratton, K. E. Thome, W. Tierens, M. Tobin, I. Uzun-Kaymak, B. Van Compernolle, J. Wai, W. Wang, W. P. Wehner, A. S. Welander, J. Yang, V. Zamkovska, X. Zhang, X. Zhu, and S. Zweben, "NSTX-U research advancing the physics of spherical tokamaks," Nucl. Fusion **64**, 112004 (2024).
[24]See https://datacommons.princeton.edu/ for a complete data set of the different equilibria employed.
[25]M. Coury, W. Guttenfelder, D. R. Mikkelsen, J. M. Canik, G. P. Canal, A. Diallo, S. Kaye, G. J. Kramer, R. Maingi, and NSTX-U Team. "Linear gyrokinetic simulations of microinstabilities within the pedestal region of H-mode NSTX discharges in a highly shaped geometry," Phys. Plasmas **23**, 062520 (2016).
[26]J. Parisi, W. Guttenfelder, A. Nelson, R. Gaur, A. Kleiner, M. Lampert, G. Avdeeva, J. Berkery, C. Clauser, M. Curie, A. Diallo, W. Dorland, S. Kaye, J. McClenaghan, and F. Parra, "Kinetic-ballooning-limited pedestals in spherical tokamak plasmas," Nucl. Fusion **64**, 054002 (2024).
[27]J. Parisi, A. O. Nelson, W. Guttenfelder, R. Gaur, J. W. Berkery, S. M. Kaye, K. K. Barada, C. F. Clauser, A. Diallo, D. R. Hatch, A. Kleiner, M. Lampert, T. Macwan, and J. E. Menard, "Stability and transport of gyrokinetic critical pedestals," Nucl. Fusion **64**, 086034 (2024).
[28]J. F. Parisi, A. O. Nelson, R. Gaur, S. M. Kaye, F. I. Parra, J. W. Berkery, K. Barada, C. Clauser, A. J. Creely, A. Diallo, W. Guttenfelder, J. W. Hughes, L. A. Kogan, A. Kleiner, A. Q. Kuang, M. Lampert, T. Macwan, J. E. Menard, and M. A. Miller, "Kinetic-ballooning-bifurcation in tokamak pedestals across shaping and aspect-ratio," Phys. Plasmas **31**, 030702 (2024).
[29]CGYRO version (git commit) employed in linear simulations was 657f714b.
[30]M. Giacomin, D. Dickinson, D. Kennedy, B. S. Patel, and C. M. Roach, "Nonlinear microtearing modes in mast and their stochastic layer formation," Plasma Phys. Controlled Fusion **65**, 095019 (2023).
[31]B. S. Patel, D. Dickinson, C. M. Roach, and H. R. Wilson, "Linear gyrokinetic stability of a high non-inductive spherical tokamak," Nucl. Fusion **62**, 016009 (2022).

[32]F. Jenko, W. Dorland, and G. W. Hammett, "Critical gradient formula for toroidal electron temperature gradient modes," Phys. Plasmas **8**, 4096–4104 (2001).
[33]T. Rafiq, Z. Wang, S. Morosohk, E. Schuster, J. Weiland, W. Choi, and H.-T. Kim, "Validating the multi-mode model's ability to reproduce diverse tokamak scenarios," Plasma **6**, 435–458 (2023).
[34]C. Bourdelle, W. Dorland, X. Garbet, G. W. Hammett, M. Kotschenreuther, G. Rewoldt, and E. J. Synakowski, "Stabilizing impact of high gradient of on microturbulence," Phys. Plasmas **10**, 2881–2887 (2003).
[35]D. Kennedy, C. Roach, M. Giacomin, P. Ivanov, T. Adkins, F. Sheffield, T. Görler, A. Bokshi, D. Dickinson, H. Dudding, and B. Patel, "On the importance of parallel magnetic-field fluctuations for electromagnetic instabilities in STEP," Nucl. Fusion **64**, 086049 (2024).
[36]T. Rafiq, C. Wilson, L. Luo, J. Weiland, E. Schuster, A. Y. Pankin, W. Guttenfelder, and S. Kaye, "Electron temperature gradient driven transport model for tokamak plasmas," Phys. Plasmas **29**, 092503 (2022).
[37]T. Rafiq, C. Wilson, C. F. Clauser, E. Schuster, J. Weiland, J. Anderson, S. M. Kaye, A. Pankin, B. P. LeBlanc, and R. E. Bell, "Predictive modeling of NSTX discharges with the updated multi-mode anomalous transport module," Nucl. Fusion **64**, 076024 (2024).
[38]G. M. Staebler and J. E. Kinsey, "Electron collisions in the trapped gyro-Landau fluid transport model," Phys. Plasmas **17**, 122309 (2010).
[39]G. Staebler, N. Howard, J. Candy, and C. Holland, "A model of the saturation of coupled electron and ion scale gyrokinetic turbulence," Nucl. Fusion **57**, 066046 (2017).
[40]In the ETGM model, the equilibrium is based on the $s-\alpha$ assumption, with the eigenfunction chosen as $\phi(\theta)=1+\cos(\theta)$ for $\theta\leq\pi$. Rather than solving the problem along the field line or ballooning angle θ, the norms of the relevant differential operators ($\langle\omega_D\rangle$, $\langle k_\parallel\rangle$, and $\langle k_\perp\rangle$) are computed directly,[44] which accelerates the eigenvalue calculations. However, this approach shifts the ETGM growth rate spectrum towards lower wavenumbers in $k_y\rho_s$, resulting in a higher ETGM diffusivity. Typically, ETG modes exhibit large k_y and smaller k_x; thus, we have assumed $k_x=\frac{1}{2}k_y$.[4] While modifying the estimation of k_x has a minimal impact on the shape of the growth rate, it significantly influences the magnitude of ETGM diffusivity. Therefore, calibrating the ETGM thermal diffusivity using experimental discharge data is necessary. The calibration procedure for ETGM involved adjusting a calibration factor applied to the diffusivity. This calibration was performed globally, based on matching the overall heat flux profile to NSTX experimental data[36] and set to 0.05 (which is applied, for example, to Eq. (21) in Ref. 36). This global calibration is applied across entire discharges and remains fixed without adjustments at individual radii, demonstrating the model's ability to capture key transport features across a broad range of conditions. The model's thermal flux, as shown in Figs. 10 and 11, incorporates this calibration, with no additional free parameters introduced. The same calibration factor is also employed when validating time-dependent temperature profiles in NSTX discharges.[37] This ETGM model should describe ETG transport in plasma regimes close to the NSTX equilibrium used for calibration, and is part of the MMM module used in TRANSP that is available for other discharges and devices.
[41]G. Avdeeva, K. Thome, S. Smith, D. Battaglia, C. Clauser, W. Guttenfelder, S. Kaye, J. McClenaghan, O. Meneghini, T. Odstrcil, and G. Staebler, "Energy transport analysis of NSTX plasmas with the TGLF turbulent and NEO neoclassical transport models," Nucl. Fusion **63**, 126020 (2023).
[42]It is noted here that the $E\times B$ flow shear definition used in ETGM differs from the one used in CGYRO. ETGM uses the Hahm and Burrel definition,[45–47] $\gamma_E=(RB_{pol}/B_{tor})\partial_r(E_r/RB_{pol})$, whereas CGYRO (and therefore TGLF) uses flux surface expression introduced by Waltz and Miller[48] and Candy and Belli[49] $\gamma_E=(r/q)\partial_r(E_r/RB_{pol})$. The values employed by ETGM were $\gamma_E=1.14\,[c_s/a]$, at $r/a=0.6$, and $0.493\,[c_s/a]$, at $r/a=0.7$, respectively.
[43]C. F. Clauser, Data for "Electron temperature gradient instability and transport analysis in NSTX and NSTX-U plasmas," (2024), see https://datacommons.princeton.edu/discovery/catalog/doi-10-34770-r2gf-9589.
[44]A. Hirose, "Effects of charge non-neutrality and finite on the electron temperature gradient mode," Phys. Plasmas **10**, 4567–4569 (2003).
[45]T. S. Hahm and K. H. Burrell, "Flow shear induced fluctuation suppression in finite aspect ratio shaped tokamak plasma," Phys. Plasmas **2**, 1648–1651 (1995).
[46]K. H. Burrell, "Effects of E×B velocity shear and magnetic shear on turbulence and transport in magnetic confinement devices," Phys. Plasmas **4**, 1499–1518 (1997).
[47]T. Rafiq, A. H. Kritz, G. Bateman, C. Kessel, D. C. McCune, and R. V. Budny, "Effect of pedestal height and internal transport barriers on International Thermonuclear Experimental Reactor target steady state simulations," Phys. Plasmas **18**, 112508 (2011).
[48]R. E. Waltz and R. L. Miller, "Ion temperature gradient turbulence simulations and plasma flux surface shape," Phys. Plasmas **6**, 4265–4271 (1999).
[49]J. Candy and E. Belli, "Spectral treatment of gyrokinetic shear flow," J. Comput. Phys. **356**, 448–457 (2018).